energies

MDPI

Article

The Consequences of Air Density Variations over Northeastern Scotland for Offshore Wind Energy Potential

Alain Ulazia [1,*], Ander Nafarrate [1], Gabriel Ibarra-Berastegi [2,3], Jon Sáenz [3,4] and Sheila Carreno-Madinabeitia [5]

1 Department of NE and Fluid Mechanics, University of the Basque Country (UPV/EHU), Otaola 29, 20600 Eibar, Spain
2 Department of NE and Fluid Mechanics, University of the Basque Country (UPV/EHU), Alda. Urkijo, 48013 Bilbao, Spain
3 Joint Research Unit (UPV/EHU-IEO) Plentziako Itsas Estazioa, University of the Basque Country (UPV/EHU), Areatza Hiribidea 47, 48620 Plentzia, Spain
4 Department of Applied Physics II, University of the Basque Country (UPV/EHU), B. Sarriena s/n, 48940 Leioa, Spain
5 Meteorology Area, Energy and Environment Division, TECNALIA R&I, Basque Country, Spain
* Correspondence: alain.ulazia@ehu.eus

Received: 7 June 2019; Accepted: 8 July 2019; Published: 9 July 2019

Abstract: Hywind-Scotland is a wind farm in Scotland that for many reasons is at the leading edge of technology and is located at a paradigmatic study area for offshore wind energy assessment. The objective of this paper is to compute the Capacity Factor (*CF*) changes and instantaneous power generation changes due to seasonal and hourly fluctuations in air density. For that reason, the novel ERA5 reanalysis is used as a source of temperature, pressure, and wind speed data. Seasonal results for winter show that *CF* values increase by 3% due to low temperatures and denser air, with economical profit consequences of tens of thousands (US$). Hourly results show variations of 7% in air density and of 26% in power generation via FAST simulations, emphasizing the need to include air density in short-term wind energy studying.

Keywords: ERA5; air density; offshore wind energy; FAST; Scotland

1. Introduction

Recently, the European Commission presented its long-term strategy for a climate-neutral economy by 2050: *A Clean Planet for All*. The achievement of these goals implies that Europe can lead the way to climate neutrality by investing into a new energy policy framework established under the *Clean Energy for All Europeans* package. This involves an important development of renewable energy sources, especially those that have already achieved a mature stage of technological and economical feasibility, like wind energy.

The Scottish regional government is committed to a full decarbonization of its energy generation system by 2020. Scotland has the highest wind resource availability in Europe, with almost a quarter of the total resources, wind energy is overtaking hydropower as the main renewable source. Despite the widespread development of wind energy currently observed in many countries, some aspects, such as more accurate estimation of wind resources and the economic feasibility of future facilities, still need further research. Among these aspects that require better characterization is the impact that the changes

in air density due to atmospheric variability at different time-scales have on the overall electric power yield of a wind farm.

The regions of the world located at high latitudes with important wind energy potential, such as Scotland, constitute good study areas for analyses at different time scales, ranging from seasonal to day–night temperature oscillations. In fact, the difference in solar radiation intensity and duration from winter to summer is stronger at these latitudes, so seasonal air density changes can also be expected to be behind the most important changes in electricity production. Additionally, in extratropical, mid-latitude regions, the frequent appearance of baroclinic low-pressure systems implies that substantial variability exists in both pressure and temperature at the two-ten day synoptic band [1–3].

The introduction of wind energy in the past has in some occcasions, raised some vociferous public opposition due to subjective reasons such as landscape aesthetics. However, currently, in Scotland there are a number of fully operational wind farms both onshore and offshore [4,5]. Furthermore, despite the initial insufficient grid infrastructure off the Scottish coast, a floating wind farm (Hywind-Scotland) has recently come into operation. Despite the heavy storms and strong winds associated, a very high capacity factor (CF) of 65% has been recorded in the first winter working [6].

The ECMWF [7] has released its more recent product, the ERA5. After having been identified in the wind energy community as a valuable tool [8], ERA5 was also adopted for this study. ERA5 provides pressure, temperature and humidity at sea level which allows calculation of local air density. Most wind farm feasibility studies ignore the impact that air density changes have on wind energy production [9,10]. Instead, a constant value around 1.225 kg/m^3 (ρ_0) is assumed at sea level while at higher altitudes, their yearly averages are used. In these cases, the average site-specific annual air density is used to select the corresponding power curve of the turbine. For instance, Air Density Calculator of The Wind Atlas Analysis and Application Program (WAsP) can be used to estimate the air density from site elevation and the annual average air temperature at the site and hub height [11].

Therefore, most feasibility studies only use wind data that are usually retrieved from anemometers [12–14], mesoscale models [15], remote sensing data, or different reanalyses [16–27]. In the particular case of the anemometers located at wind turbines, only wind speed is measured. However, an alternative calibration of cup anemometers should be carried out to consider the impact that air density oscilations have in the drag force exerted on the cups [28].

The effect of air density has been sporadically studied in recent literature [29–32], but only at given locations and specific wind farms, without a general spatio-temporal analysis in order to see the behavior of these fluctuations due to air density in different areas of a given region. However, recent studies by the current authors in the Gulf of Biscay and the Mediterranean region and by other researchers in Japan suggest that air density may have an important impact on seasonal and daily energy production, considering its effect on normalized wind speed [33–35].

In fact, air densities lower than the standard sea-level value may require a complete redesign of the wind turbine blades, for example for wind turbines located at high altitudes [36,37]. As a paradigmatic example, Farkas et al. [29] analyzed the temporal variations in air density at a specific location and proposed a correction to the regular power curve of a wind turbine. The air density variations around the mean reached 15%. This figure is far from negligible, since wind power density changes are proportionally driven by air density changes, and energy production losses in wind farms due to important mechanical problems such as pitch misalignment can reach comparable values [38]. Similarly, Collins et al. [30] showed that the difference in electric yield between a hot day and on a cold day can be of a similar order of magnitude (10%) for medium-range speeds below the rated wind speed and also, above the cut-in wind speed.

The possibilities for a widespread implementation of offshore wind energy have multiplied due to the recent development of floating wind farms, such as the aforementioned Hywind-Scotland wind farm [39]. Further technological solutions in the field of deep-water mooring and transportation of electricity to the mainland grid can pave the way to an widespread implementation of offshore wind energy. Such development will require a proper evaluation of the true wind energy potential at the

specific offshore locations so that an accurate estimation of costs and economic feasibility can be known beforehand. In this context, the impact that changes in air density at different time scales have on the final electric production needs to be correctly evaluated.

Recently, Floors et al. [10] have published a contribution in this line mentioning the importance of air density in wind energy potential estimation, but in their case the main contribution is about the computation of reduction of air density at the hub height compared to air density obtained from temperature, pressure and humidity measurements at lower levels. Additionally, they have found that using re-analysis data (ERA5 like in this work) to estimate air density gives similar or smaller errors compared to using nearest measurements around the point of study. A method to interpolate power curves that are valid for site-specific air densities is also presented, but their objective is not to focus on temporal variations and they use annual averages to find the corresponding power curve. Other very recent publications also ignores these seasonal variations and consider the effect of geographical altitude or humidity in air density and the consequent wind energy production [40,41].

In this study, the seasonal and intra-day air density changes and their impacts on wind energy production off the Scottish coast are shown, with a more specific focus on Hywind project. Additionally, in this study, extreme cases will be analyzed as well as the differences between winter and summer production, instantaneous power generation using the FAST simulator, and other important aspects of wind energy fluctuations due to air density.

2. Data and Methodology

2.1. Data

2.1.1. The ERA5 Reanalysis and the Study Area

The European Centre for Medium-Range Weather Forecasts (ECMWF) (https://www.ecmwf.int/) recently developed the ERA5 reanalysis [7]. It is freely available to the scientific community through the Copernicus Climate Data Store (https://cds.climate.copernicus.eu/). ERA5 provides hourly values corresponding to a great number of atmospheric and oceanic variables at a spatial resolution of 31 km. For this study, the ERA5 hourly values of the following variables were retrieved from the ECMWF: surface level pressure, temperature at 2 m, and wind values at 10 and 100 m above ground level. The wind values are expressed as the zonal (U_{10} and U_{100}) and meridional (V_{10} and V_{100}) components of the wind vector. These values must be adapted to have the air density and the wind speed module at the hub height.

Before ECMWF released ERA5 and made it public, the authors conducted several studies with their own integrations using the the Weather Research and Forecasting (WRF) meteorological model with data assimilation [33,34] nested into the previous coarser-resolution ERA-Interim reanalysis [42]. Nevertheless, currently, ERA5 provides a resolution high enough for wind energy studies, and the authors have successfully used ERA5 for technical purposes, such as for the identification of defective anemometers at wind farms [43]. Additionally, the potential of ERA5 has already been stressed in recent publications with a myriad of applications, such as wind energy resource assessment, economical constraint, or wave–wind interactions in offshore wind farms [8,44–49]. To summarize, ERA5 is widely accepted as a reliable source of data for wind energy assessment studies and was also used in this work. The next reanalysis, with an even higher resolution, ERA6, is scheduled to be released in 2020 (https://confluence.ecmwf.int/display/CKB/What+is+ERA5).

In addition, the authors have recently developed *aiRthermo*, an *R* package for the calculation of several features related to the water cycle in the atmosphere [50,51]. In the present study, *aiRthermo* was used to estimate the impact that humidity changes may have on air density. The results can be seen in Figure 1 where the behavior of the air density ratio (moist air density versus dry air density at 20 °C) for a range of ambient temperatures and different values of relative humidity can be seen. Extremely hot temperatures and very high humidity levels are necessary to reach a ratio of 0.95, where the difference between dry air density and 100% humid air density is below 5%. At average temperatures of around 20 °C, this difference is around 0.1%. For the study area, this can be expected to be the case for seasonal

or yearly analyses based on average values. This is in agreement with previous works by authors for other environments [52] where the effect of humidity on air density has also been acknowledged as negligible. All of these scientific results led us to ignore its effects in this paper too and to the use of the Equation (2) for dry air density.

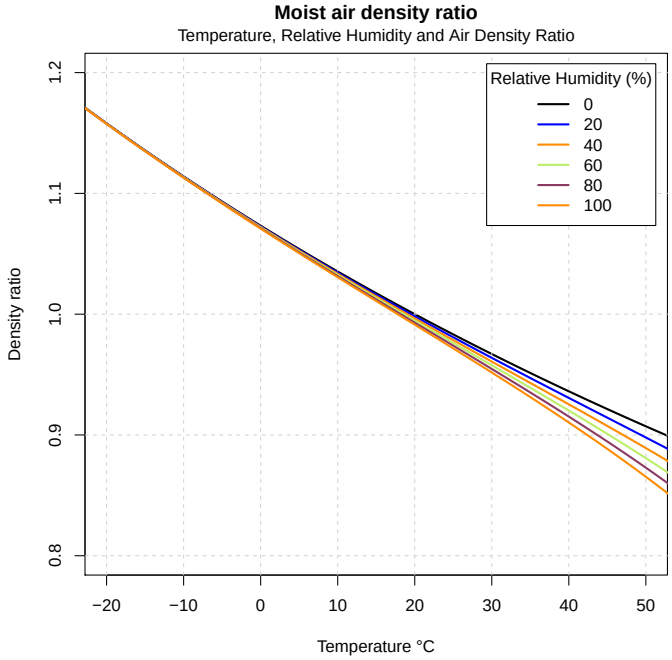

Figure 1. Moist air density ratio versus temperature and relative humidity.

Figure 2 shows the study area. The ERA5 gridpoints are represented on the map, and hourly data corresponding to the 2008–2017 period was used (87,648 cases at each gridpoint). Although monthly means are used to represent seasonal maps, an extreme-case analysis was carried out using hourly data. Hywind-Scotland Pilot Park is also shown ($-1.36°$, $57.48°$) and was used for a particular final case study. Each pixel is around 31 km in latitude, and the location analyzed is at a distance of around 500 km from the coast.

2.1.2. SIEMENS 154/6 Floating Wind Turbine

The SIEMENS 154/6 floating wind turbines located at the Hywind-Scotland farm have a diameter of 154 m, a hub height of 178 m, with a rated power of 6 MW. Among many other variables, ERA5 provides wind speed data at 10 and 100 m above sea level. The wind speed values change vertically with heigth according to a logarithmic law. At a first step sea surface roughness (z_0) can derived by solving (Equation (1)) using a wind speed at 10 and 100 m. The typical values were around 0.0002–0.0005 m, an usual value for calm sea-surface roughness [9]. At a second step (z_0) and wind speed at 100 m can be introduced in (Equation (1)) and then wind speed at 178 m $U(178)$ can be obtained. Despite the internal contributions of the assimilation algorithms used in ERA5 which carefully compute the interaction with the surface at different model heights (version Cy41R2 of the Integrated Forecasting System (IFS) by ECMWF [53]), the current procedure ignores partially the important issue on the stability of the atmosphere. For instance, WAsP contains a stability model which employs separate mean and heat flux values for different conditions that can be used in more accurate studies in the future [11].

$$\frac{U(100)}{U(10)} = \frac{log(100/z_0)}{log(10/z_0)} \Rightarrow z_0 \Rightarrow \frac{U(178)}{U(10)} = \frac{log(178/z_0)}{log(10/z_0)} \Rightarrow U(178). \quad (1)$$

Henceforth, the wind speed estimated at 178 m $U(178)$ is denoted as U.

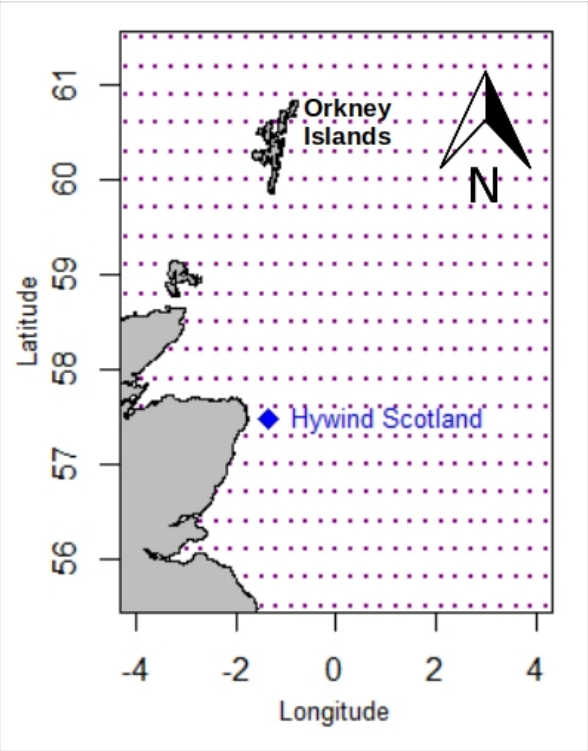

Figure 2. Study area and ERA5 gridpoints over Northeastern Scotland.

2.2. Methodology

2.2.1. Air Density

The air density was calculated using Equation (2) as a function of the pressure (P) and temperature (T) at the hub height:

$$\rho = \frac{P}{R_d T} \tag{2}$$

where R_d = 287.058 J/kg K, the constant of the ideal gases for dry air.

In order to compute the air density at the hub height the correction method recently presented by Floors et al. [10] have been used. This method is based on the hydrostatic model of the atmosphere and uses the US standard atmosphere model to evaluate the reduction of temperature and pressure with height [54]. Correcting the surface values to hub height yields a nearly 2% reduction in air density. This correction does not affect the relative changes in percent of air density, wind power density and capacity factor (see $\Delta\rho$, ΔWPD, and ΔCF), because the reduction is the same for the instantaneous event or for the average value, but it affects the absolute values (e.g., Table 1).

Table 1. Summary of statistical indicators for ρ and ΔWPD.

Stat. Ind.	ρ (kg/m^3)	ΔWPD (%)
Min.	1.15	−7.1
1rst qu.	1.21	−1.2
Mean	1.23	–
3rd qu.	1.25	1.8
Max.	1.33	8.9

Another important contribution of Floors et al. [10] is about the lapse rate that gives the lineal reduction of temperature with height for different latitudes based on ERA5 data. According to the Figure 3 of this publication, at the latitudes of Scotland around 50°, the lapse rate is lower than the US

standard of -0.0065 K/m, and it is around -0.0050. This means that the reduction of temperature at hub height is lower than the value given by the standard lapse rate, and therefore, the air density variation due to temperature is also smaller. However, the US standard is used to establish an upper limit of reduction.

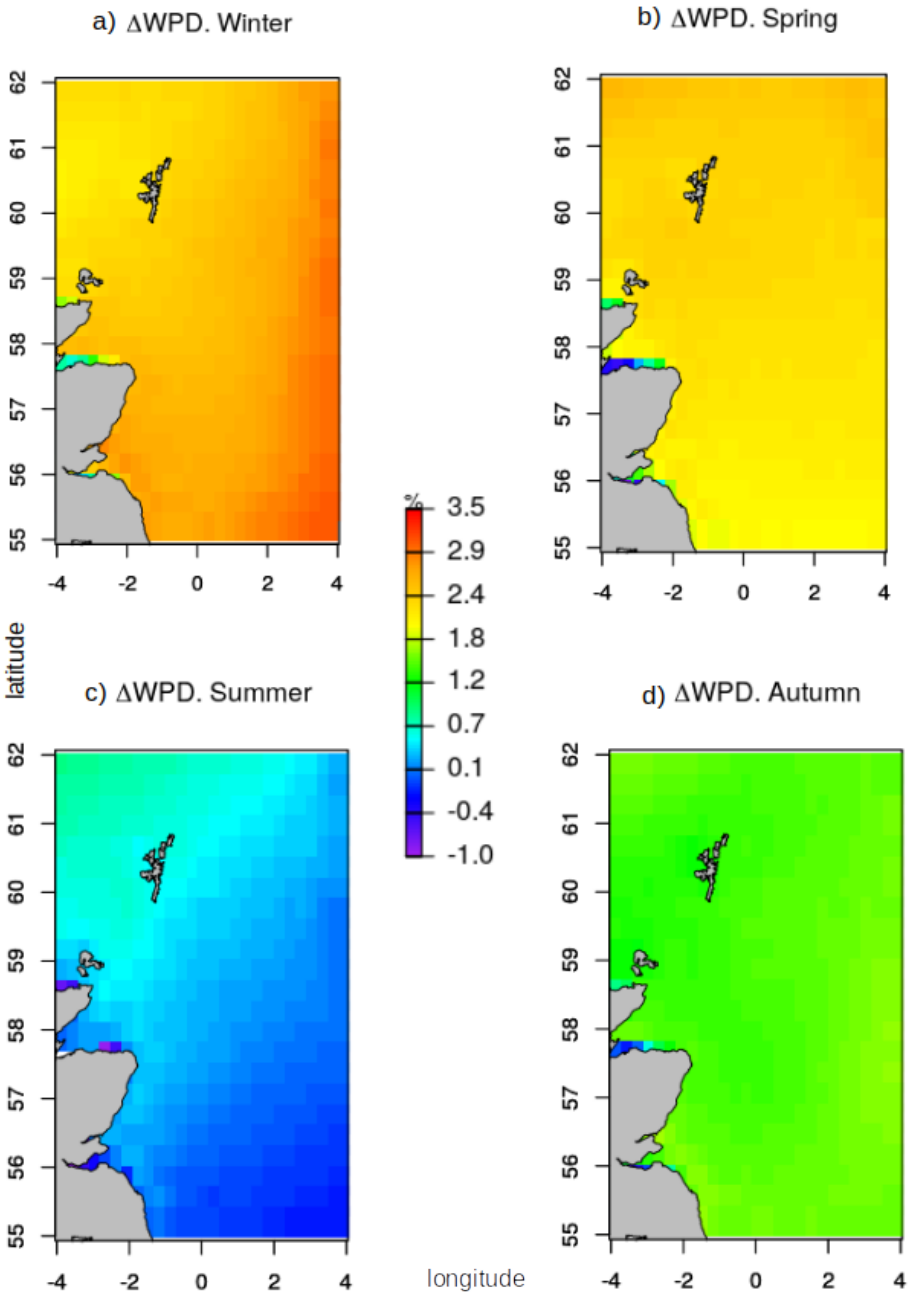

Figure 3. ΔWPD in percentage terms for the four seasons in the study area: (**a**) winter; (**b**) spring; (**c**) summer; and (**d**) autumn.

Therefore, the departure of air density from the regular value of $\rho_0 = 1.225$ kg/m^3 can be expressed in percentage terms using Equation (3):

$$\Delta\rho = 100 \times \frac{(\rho - \rho_0)}{\rho_0} \tag{3}$$

As explained above, the effect of humidity in the air density values was ignored.

2.2.2. Normalization of the Wind Speed According to Air Density

Instead of the usual hypothesis that emphasizes that the power production of the turbine is the same at a given wind speed, the corrected hypothesis involves both air density and wind power density (WPD), assuming that the power production of the turbine is the same for a constant WPD. Thus, WPD is defined as the kinetic power of the wind per unit area [W/m^2] using air density (ρ) and wind speed U according to Equation (4).

$$WPD = \frac{1}{2}\rho U^3 \tag{4}$$

If the constant average air density at the location and the real air density are ρ_0 and ρ, respectively, and U and U_n denote the real and normalized wind speeds, the hypothesis establishes that the power production will be the same if WPD remains unchanged (Equation (5)):

$$WPD_0 = WPD \Rightarrow \frac{1}{2}\rho U^3 = \frac{1}{2}\rho_0 U_n^3 \tag{5}$$

Thus, the normalized wind speed is derived from this expression, and its value has been adopted and is recommended by IEC 61400-12 [55] according to Equation (6):

$$U_n = \left(\frac{\rho}{\rho_0}\right)^{1/3} U \tag{6}$$

2.2.3. Capacity Factor and Energy Production

The overall electricity production for a given period can be estimated by using the observed wind speed values as inputs for the turbine's power curve and aggregating the electric outputs for the period considered. With the same purpose of estimating the electric production of a wind turbine, a more simple and straightforward equation, namely the Master's equation, can be found in the literature [9,56]. It has been largely used by authors [33,34,38], and for a given period and turbine, it provides the capacity factor (CF), the ratio between the real annual energy production and the ideal production (working all hours of the year at a rated power). The (CF) is calculated as a function of the local mean wind speed, rated power (P_R in kW), and turbine diameter (D) (Equation (7)):

$$CF_n = 0.087\bar{U}_n - \frac{P_R}{D^2} \tag{7}$$

In this work, the Master's equation has been used to compare the capacity factors obtained in two ways:

1. Using the normalized wind speed from Equation (6) and therefore, incorporating the effect of air density changes (CF_n); and
2. Using the observed wind speed associated with a constant ρ value of 1.225 kg/m^3 (CF).

The difference between both represents the variation in the capacity factor attributable to air density variations: $\Delta CF = CF_n - CF$. In this paper, all four seasons were considered (Summer, JAS; Autumn, OND; Winter, JFM; Spring, AMJ), and seasonal differences in CF were calculated for these four seasons. Thus, the seasonal energy production differences in MWh attributable to air density changes (ΔSEP) can be assessed from the Master's expression after incorporating the number of hours into Equation (8): $P_R = 6$ MW for the selected turbine SIEMENS 154/6.

$$\Delta SEP = (CF_n - CF) \times P_R \times 365.25 \times 24 \times \frac{1}{4} \tag{8}$$

2.2.4. Analysis at Hywind-Scotland's Nearest Gridpoint

ERA5 hourly records at the nearest gridpoint, located 16 km from Hywind wind farm, corresponding to the 2008–2017 period were used. The nearest neighbor approach is commonly used for fields which vary substantially [57,58] because, otherwise, bilinear interpolation tends to smooth too much the resulting interpolated field, particularly if these fields are not very smooth [59]. In our case, since the spatial autocorrelation of some of the variables is not very high, we find it safer to use the nearest neighbor technique. This is a methodology a commonly used for this purpose; see for instance [60–62] for a couple of examples which use the nearest neighbor technique. We find this safer for areas (such as coastal ones) where some model gridpoints might be surrounded by close ones from land areas in case bilinear interpolation was used.

In this work, using this database, the impact of air density on electric production was analyzed at two different time scales:

1. The hourly historical maximum and minimum air density values and their percentage variations with respect to the historical average value ($\Delta minM_\rho$ and $\Delta maxM_\rho$). Equation (9) shows the definition of $\Delta maxM_\rho$ given the historical maximum (ρ_{max}) and its mean ($\bar{\rho}$). The definition of $\Delta minM_\rho$ would be equivalent:

$$\Delta maxM_\rho = \left(\frac{\rho_{max}}{\bar{\rho}} - 1\right) \times 100 \tag{9}$$

2. Since hourly values are used, the intra-daily evolution of air density and effects such as the day–night cycle or land–sea breezes can be properly characterized. The characterization of cycles below 24 h is important, because 24 h is the leading studying horizon for wind energy farms [63]. A new parameter of deviation was defined, and the percentage deviation of the ratio between the minimum air density of the day d (ρ^d_{min}) and the maximum air density value of the day d (ρ^d_{max}) was used for that (Equation (10)):

$$\Delta\rho_{day} = \left(\frac{\rho^d_{max}}{\rho^d_{min}} - 1\right) \times 100 \tag{10}$$

2.2.5. Instantaneous Power Production Using FAST Simulations

Both aspects of the previous section were also studied in the context of the instantaneous power produced by the turbine at a given moment. For that reason, the time scale of the analysis needed to be finer (in centiseconds), and simulators such as FAST of NREL were used considering the pitch control, the turbulent wind flow on the actuator disk, and other complex elements that constitute the turbine's actual power abortion (see https://nwtc.nrel.gov/FAST).

FAST code [64] was implemented on the NREL's 5 MW reference offshore turbine, which is the most similar option to the 6 MW turbine of Hywind farm. This code presents options for floating or bottom-fixed offshore and onshore turbines, and its results have been validated in various recent studies [65–67].

The highest and lowest air densities in the study period were used for comparison, together with the average air density. A mean wind speed value of 8.2 m/s was used for the three simulations. It must be taken into account that this wind speed is in the U^3 zone of the power curve of a turbine and that the real power curve can be more affected by the air density changes here than in the rated power zone.

First, the simulator creates a turbulent signal around the mean wind speed on a 15 × 15 grid over the plane of the actuator disk. This is the input of the FAST code which is run on a 100 s time series, changing the air density in the aerodynamic package and activating the usual pitch control. It should be noted that the outputs during the first 30–40 s correspond to an intermediate stage before the algorithm converges to a solution. Although Octave/Matlab (see https://www.gnu.org/software/octave/) can

represent the time evolution of several output parameters, only the time series of the instantaneous power was studied for the two extreme and the mean air density. The objective was to assess the power production differences between the two extremes of air density while keeping the average wind speed corresponding to the location constant.

3. Results

3.1. Map Representations

3.1.1. Seasonal Variations

Figure 3 shows the changes in wind power density ΔWPD expressed in percentage terms for the four seasons. Seasonal changes in density $\Delta\rho$ are not shown, although they follow a similar pattern. The color scale of the plots is the same for the four maps so that comparisons are straightforward. The WPD oscilations in summer (c) are negative but not very high in absolute terms, if compared with the WPD given by the regular ρ_0. This can be seen mainly in the Southern part of the map and in the open ocean, as could be expected from Equation (2). Figure 3a shows a similar result for winter. The increase in air density due to low temperatures is relevant: it almost reaches 3.5% in the open ocean and 2–3% near shore, with the lowest increments under the influence/wake of Orkney island. Spring (b) and autumn (d) show intermediate values without relevance for this study. Thus, only maps for winter and summer are shown in the next sections.

The variation of in the capacity factor ΔCF defined in Section 2.2.3 for summer and winter shows an analogous spatial behavior in the ΔWPD maps. In Figure 4, almost irrelevant variation can be seen for summer and a relevant ΔCF of 1% can be seen for winter with a weak increment towards the south. The reader should note that ΔCF's percentage value is an absolute difference and not a relative one ($\Delta CF = CF_n - CF$).

Applying Equation (8) for ΔSEP, the variation of seasonal energy production, this 1% means an increment of 131 MWh for winter considering the above-mentioned 6 MW turbine of Hywind-Scotland.

3.1.2. Maximum to Mean and Minimum to Mean Air Density Ratio Oscillations

Figure 5 shows the spatial pattern of the minimum to mean ratio and the maximum to mean ratio as percentages. The $\Delta minM_\rho$ variation range is from -7% to -5% with the strongest values in the northwestern part of the Orkney islands. On the other hand, $\Delta maxM_\rho$ shows very strong values of 12% near shore, but the common variations in the sea are between +4% and +7%, with the strongest variations at the lowest latitudes. This implies a general variation interval of around 10–14%, a very relevant percentage which is proportional for WPD if the estimation of wind power is based on the assumption of a constant average air density at each location.

The extreme values of 7% around the average air density represent $(1.07)^{1/3} = 1.02$, an increase of 2% for the hourly normalized wind speed U_n. The impact of these wind speed deviations in the electric power generated is most influential in the U^3 zone of the power curve, that is, the region with the greatest slope. Figure 6 shows this effect qualitatively, in which the vertical axis of power can be limited by the Siemens 6 MW turbine (the cut-in and rated wind speed of the NREL 5 MW turbine is also very similar). As a result, similar changes in air density tend to result in more intense changes in electric power with low average wind speed values.

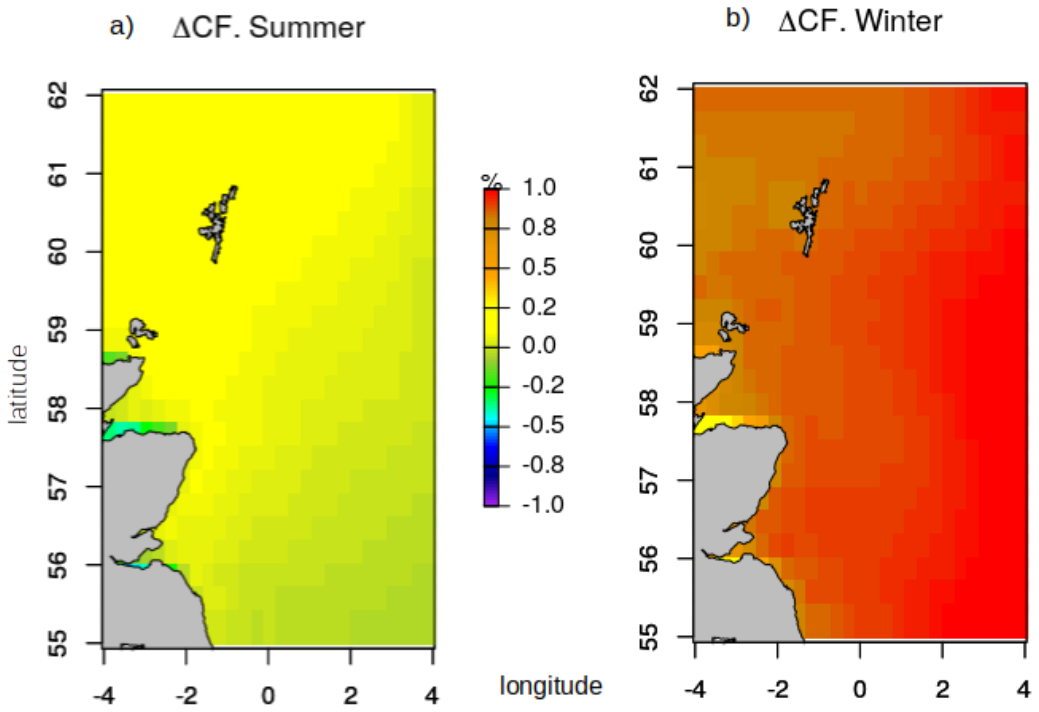

Figure 4. Changes in the capacity factor (ΔCF) in percentage terms in the study area: (**a**) summer; (**b**) winter.

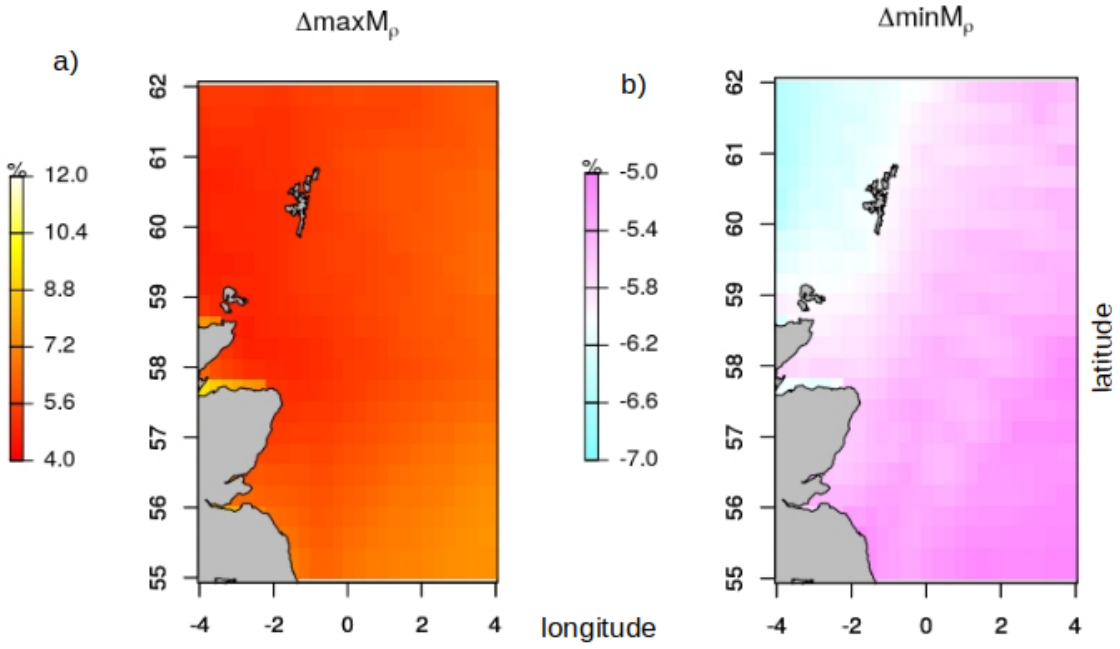

Figure 5. (**a**) Minimum to mean air density variation $\Delta minM_\rho$; (**b**) maximum to mean air density variation $\Delta maxM_\rho$ in the study area.

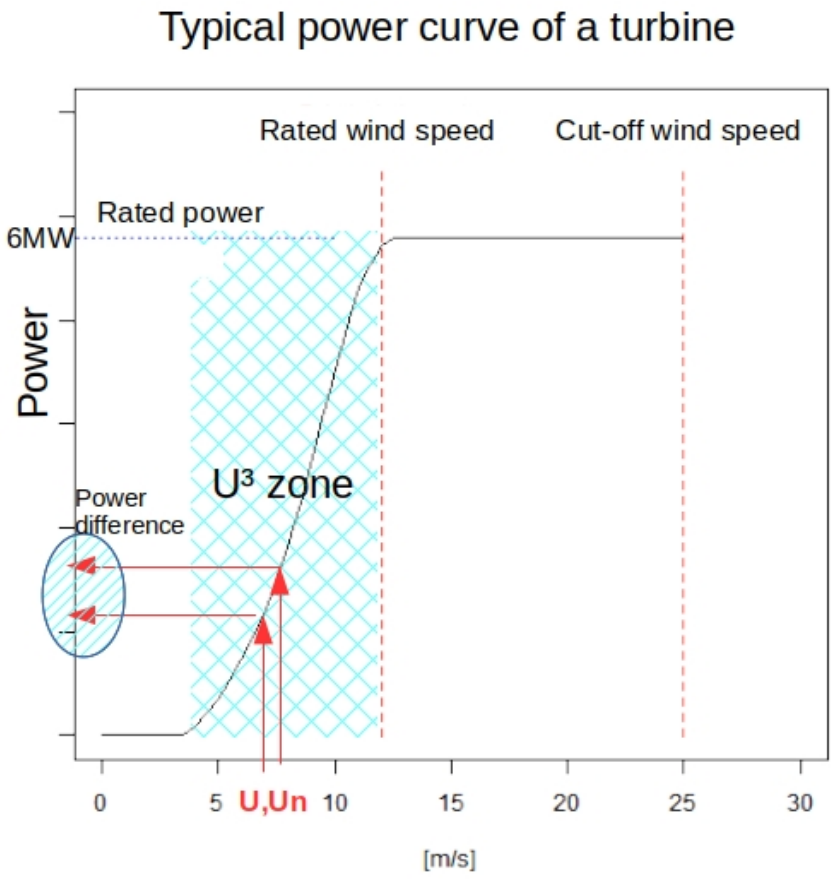

Figure 6. The normalized wind speed U_n and the U in the U^3 zone of a typical power curve and the subsequent considerable power increase.

In addition, the differential $d(U^3) = 3U^2dU$ gives a first estimation of the relative error of the power $\Delta P/P$ with respect to the relative error in the wind speed, which should be multiplied by three (Equation (11)):

$$\frac{\Delta P}{P} = \frac{3U^2\Delta U}{U^3} = 3\frac{\Delta U}{U}. \tag{11}$$

This means that a variation of 2% or 3% in wind speed due to normalization via the real air density implies a variation of 6% or 9% in power. However, this is a first estimation, and it will be shown (Section 3.3) that an aeroelastic simulator with active pitch control of the turbine gives even higher deviations in power.

3.2. Particular Case at Hywind Scotland

A particular focus has been given to the nearest ERA5 gridpoint to Hywind-Scotland wind farm, at a distance of only 16 km. An in-depth analysis of hourly records from this gridpoint was carried out and means, quartiles, and extremes of air density and associated instantaneous WPD oscillations were computed (See Table 1).

The difference between the minimum and maximum cases is 0.18 kg/m^3, around 15% of the average value. Due to the direct proportionality between air density and WPD, this range is similar as for WPD, with oscillations between −7% and + 8.9% with respect to the average. This higlights how important the impact that changes of air density in the energy production may be.

When daily air density variations were analyzed, the results were also relevant. Figure 7 shows the daily time series of air density oscillations ($\Delta\rho_{day}$) in the study period of ERA5 at Hywind-Scotland

pilot park's nearest gridpoint. The variation in the maximum air density with respect to the minimum on each day exhibits a low average of 1.4%, but there are a few extreme cases that exceed 5%. The most extreme record took place on 9 December 2014, when a value of 5.5% was reached. The variation in temperature was not important (from 3.2 °C at night to 11.3 °C in the afternoon), but the pressure dropped significantly from 1021 to 996 mb due to the arrival of a storm. Thus, it seems that, for variations in daily air density, the main cause is pressure and not temperature, as in the case of seasonal air density changes.

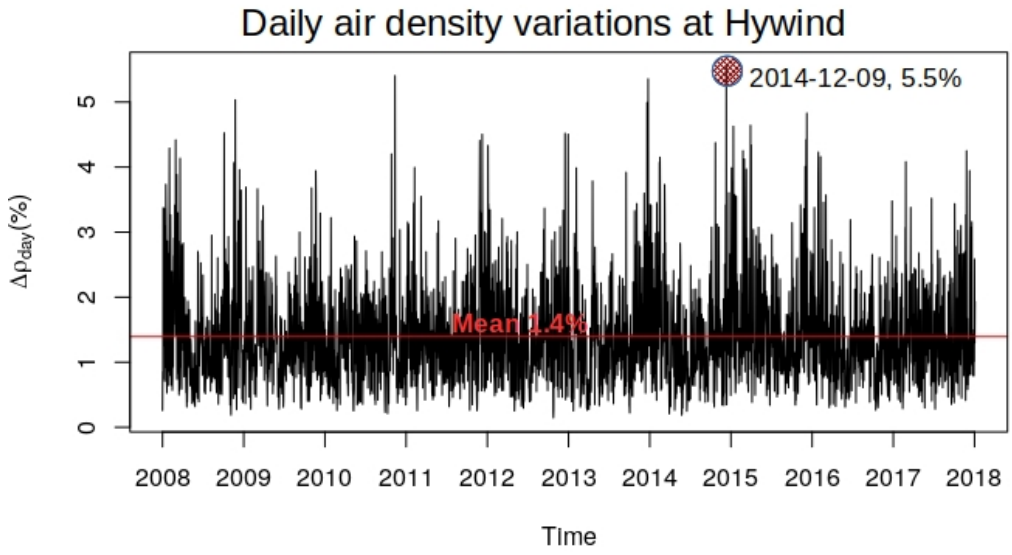

Figure 7. Daily time series of air density variations at Hywind-Scotland.

3.3. Simulation Using FAST

The minimum, maximum, and mean values of air density shown in Table 1 were used to develop a FAST simulation of the average wind speed at Hywind-Scotland (8.2 m/s). Figure 8 shows the power time series of the three simulations with the stabilization zone on the left due to the reaction of the pitch control and other regulation aspects of the turbine from the initial conditions. After 30–40 s, the FAST algorithm converges to a power value around 2 MW with subsequent small oscillations around this value due to the turbine regulation effects. For the different air density values considered, a variation of 26% can be observed around the mean air density curve, with a similar deviation of 12–13% above (high air density of 1.33 kg/m^3) and below (low air density of 1.15 kg/m^3) it. These values are near the ones estimated in the error estimation presented in Equation (11), although they are slightly higher.

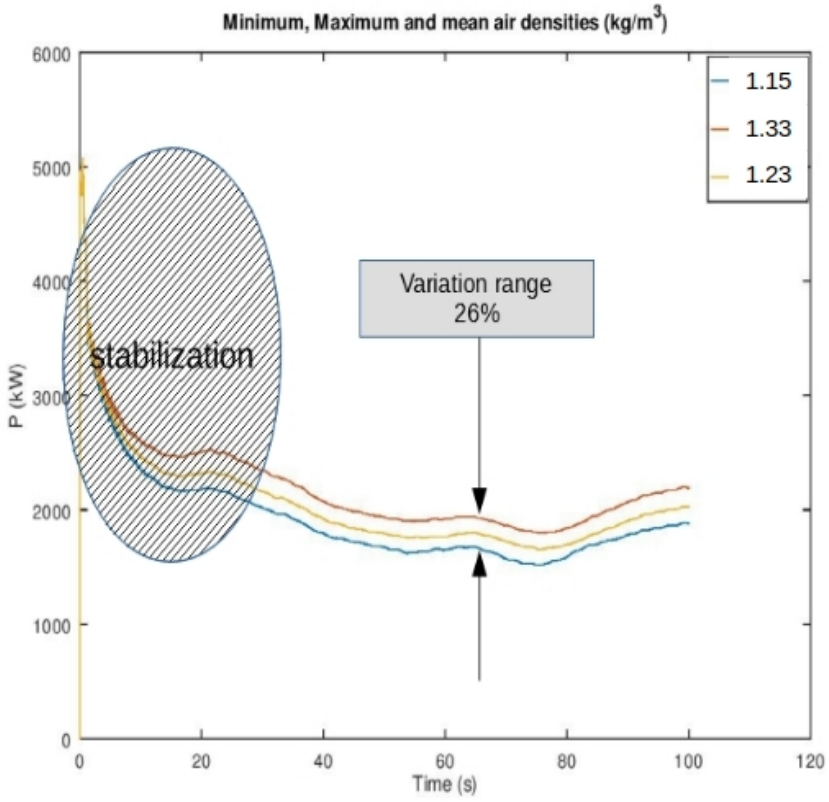

Figure 8. Simulation using FAST for the minimum, maximum, and mean air density values for the average wind speed at Hywind-Scotland.

4. Discussion

There are several interesting points that can be debated based on the results:

1. It has been shown that the observed variation of 2–3% for WPD due to air density fluctuations in winter implies a subsequent ΔCF of 1%. Thus, one turbine of 6 MW will produce 131 MWh more energy in winter than that estimated by the average air density at the site [11], which corresponds to 7860 US$ if a typical COE of 0.06 US$/kWh in wind energy is assumed [9]. This deviation of 1% is characteristic in Scottish waters, although variations from summer to winter can be higher. Besides, these economical deviations are approximately proportional to the nominal power of the considered turbine, and the most powerful turbines of the market (around 12 MW) would therefore, duplicate the profit in winter.
2. By analyzing the impact that air density changes have in the instantaneous power generation described by the power curve of the turbine using hourly data, locations with maximum increments of 7% with respect to the average were found in the study area (see maps in Figure 5). The cubic root law of the normalization technique implies an increment of 2–3% for wind speed, which should be multiplied by three if the error in power is computed (Equation (11)). These estimated deviations that are near 10% in the U^3 zone of the power curve (see Figure 6) were corroborated using advanced simulations with the aeroelastic code FAST, as presented in Section 3.3.
3. The maximum variations in air density within a given day at Hywind-Scotland show extreme cases that overcome the 5% with respect to the minimum of the day. These values are in the range within the order of magnitude of the previous historical maximum case, which imply similar power deviations. Instead of the seasonality of temperature, in the case of these daily fluctuations, sudden drops of pressure have been identified as the cause of strong air density changes.

4. Events occurring within 24 h are very important for the wind energy industry, since the typical studying period is around this time range [63]. Thus, instead of only focusing on the provision of wind speed, the results of this work also indicate the necessity of air density short-term studies (pressure and temperature) for the wind industry.
5. This aspect is also stressed for the Hywind-Scotland case, where in historical extreme cases, the instantaneous air density went from 1.17 to 1.35 kg/m^3, with almost proportional fluctuations in WPD around the mean.
6. Energy production losses in wind farms due to important mechanical or aerodynamic problems, such as pitch misalignment, present similar deviations [38]. Hence, the cause of energy production deviations can be confused with technical issues instead of related to questions about the wind resource and air density fluctuations.

5. Conclusions and Future Outlook

ERA5 is the latest climate reanalysis produced by the ECMWF, and has become a powerful source of meteorological data. It covers the whole planet, and any study area can be selected to develop a wind energy feasibility study considering all of the involved parameters, not only the wind speed [8]. By means of ERA5, a method of characterizing the deviations due to air density fluctuations in WPD, CF, and instantaneous power generation was presented. High frequencies power changes due to rapid air density oscillations can be also estimated using hourly data at a specific location. Expressed in electric generation terms the summer–winter overall variation intervals can reach 2–3% and even up to 26% for maximum–minimum differences in instantaneous power accurately computed by aeroelastic codes, with economical consequences for one turbine production that can reach tens of thousands of US$. Besides this, strong air density fluctuations can also occur within the daily scale. Thus, the study of air density should be included in wind energy short-term studies. Finally, these short-term variations distort the real power curve in the U^3 zone, an effect that can be mixed up with other technical problems such as pitch misalignment or control and regulation faults [38].

The methodology presented here is not exclusive to offshore areas, and it could also be applied onshore. However, onshore farms in complex terrain may well require a finer spatial resolution, specially in complex terrain areas. For that objective, in the future, data from meteorological models, such as WRF with data assimilation nested into ERA5 can be applied, as was done in previous papers by the current authors [33,34].

The important result of Floors et al. [10] about the behavior of the lapse rate versus different latitudes could also be interesting in the future to study the effect of air density in wind energy production around regions at different latitudes in the world. This planetary variation of the lapse rate is very relevant at very high latitudes near the Arctic and the Antarctic, where its value can be near zero or even positive, without a reduction of temperature with hub height. This further affects air density reduction, because it only depends on the pressure reduction with height.

Moreover, it would be interesting to study other areas with high wind energy potential in the world that are located at different latitudes and climates. The seasonal air density changes would be weaker at equatorial latitudes, but daily pressure changes could be stronger. Along the same line, the strong daily temperature oscillations in deserts with high wind energy potential, such as the Gobi desert [68], constitute a great future topic of study. Further research is currently being carried out by the authors along these lines.

Author Contributions: Conceptualization, A.U., A.N.; Methodology, A.U.; Software, A.U., A.N.; Investigation, A.U., G.I.-B., J.S.; Writing, Review & Editing, all the authors; Supervision, all the authors; Project Administration, G.I.-B.; Funding Acquisition, G.I.-B. and J.S.

Funding: This work was financially supported by the Spanish Government through the MINECO project CGL2016-76561-R, (MINECO/ERDF, UE) and the University of the Basque Country (UPV/EHU, GIU 17/002). ERA5 hindcast data were downloaded at no cost from the Copernicus Climate Data Store. All the calculations and plots were made using *R*: https://www.r-project.org.

Conflicts of Interest: The authors declare no conflict of interest.

Abbreviations

The following abbreviations are used in this manuscript:

ECMWF	European Centre for Medium-Range Weather Forecasts
WAsP	Wind Atlas Analysis and Application Program
WRF	Weather Research and Forecasting Model
AEP	Annual Energy Production (GWh)
CF	Capacity Factor (%)
CF_n	Capacity Factor computed with normalized wind speed (%)
COE	Cost of Energy ($/KWh)
D	Wind turbine diameter (m)
$maxM_\rho$	Maximum to mean ratio of air density (%)
$minM_\rho$	Minimum to mean ratio of air density (%)
P	Surface pressure (Pa)
P_R	Rated power of the wind turbine (kW)
SEP	Seasonal Energy Production (GWh, MWh)
T	Temperature (K)
U	Wind speed (m/s)
U_n	Normalized wind speed (m/s)
WPD	Wind Power Density (W/m^2)
ΔCF	Variation of CF (in percentage, %)
ΔSEP	Change in SEP (in percent, %)
ΔWPD	Relative change in Wind Power Density (in percent, %)
$\Delta\rho$	Change in air density (in percent, %)
$\Delta\rho_{day}$	Change between maximum and minimum air density within a given day (in percent)
ρ^d_{max}	Maximum air density in the day d (kg/m^3)
ρ^d_{max}	Minimum air density in the day d (kg/m^3)
ρ	Air density (kg/m^3)
ρ_0	Standard air density (1.225 kg/m^3)

References

1. Grotjahn, R. *Global Atmospheric Circulations: Observations and Theories*; Oxford University Press: Oxford, UK, 1993; p. 450.
2. James, I.N. *Introduction to Circulating Atmospheres*; Cambridge University Press: Cambridge, UK, 1994; p. 422.
3. Vallis, G.K. *Atmospheric and Oceanic Fluid Dynamics. Fundamentals and Large-Scale Circulation*; Cambridge University Press: Cambridge, UK, 2006; p. 745.
4. Warren, C.R.; Birnie, R.V. Re-powering Scotland: Wind farms and the 'energy or environment?' Debate. *Scott. Geogr. J.* **2009**, *125*, 97–126. [CrossRef]
5. O'Keeffe, A.; Haggett, C. An investigation into the potential barriers facing the development of offshore wind energy in Scotland: Case study–Firth of Forth offshore wind farm. *Renew. Sustain. Energy Rev.* **2012**, *16*, 3711–3721. [CrossRef]
6. Statoil Company. Technical Report. 2016. Available online: https://www.statoil.com/en/news/hywindscotland.html (accessed on 20 November 2016).
7. Hersbach, H. The ERA5 Atmospheric Reanalysis. In *AGU Fall Meeting Abstracts*; American Geophysical Union: Washington, DC, USA, 2016.
8. Olauson, J. ERA5: The new champion of wind power modelling? *Renew. Energy* **2018**, *126*, 322–331. [CrossRef]
9. Manwell, J.F.; McGowan, J.G.; Rogers, A.L. *Wind Energy Explained: Theory, Design and Application*; John Wiley & Sons: Hoboken, NJ, USA, 2010.
10. Floors, R.; Nielsen, M. Estimating Air Density Using Observations and Re-Analysis Outputs for Wind Energy Purposes. *Energies* **2019**, *12*, 2038. [CrossRef]

11. Mortensen, N.G. *46200 Planning and Development of Wind Farms: Wind Resource Assessment Using the WAsP Software*; DTU Wind Energy: Lyngby, Denmark, 2015.
12. Monteiro, C.; Bessa, R.; Miranda, V.; Botterud, A.; Wang, J.; Conzelmann, G. *Wind Power Forecasting: State-of-the-Art 2009*; Technical report; Argonne National Laboratory (ANL): Lemont, IL, USA, 2009.
13. Weisser, D. A wind energy analysis of Grenada: An estimation using the Weibull density function. *Renew. Energy* **2003**, *28*, 1803–1812. [CrossRef]
14. Gökçek, M.; Bayülken, A.; Bekdemir, Ş. Investigation of wind characteristics and wind energy potential in Kirklareli, Turkey. *Renew. Energy* **2007**, *32*, 1739–1752. [CrossRef]
15. Jiménez, P.A.; González-Rouco, J.F.; García-Bustamante, E.; Navarro, J.; Montávez, J.P.; de Arellano, J.V.G.; Dudhia, J.; Muñoz-Roldan, A. Surface wind regionalization over complex terrain: Evaluation and analysis of a high-resolution WRF simulation. *J. Appl. Meteorol. Climatol.* **2010**, *49*, 268–287. [CrossRef]
16. Dvorak, M.J.; Archer, C.L.; Jacobson, M.Z. California offshore wind energy potential. *Renew. Energy* **2010**, *35*, 1244–1254. [CrossRef]
17. Gross, M.S.; Magar, V. Offshore wind energy potential estimation using UPSCALE climate data. *Energy Sci. Eng.* **2015**, *3*, 342–359. [CrossRef]
18. Akdağ, S.A.; Güler, Ö. Evaluation of wind energy investment interest and electricity generation cost analysis for Turkey. *Appl. Energy* **2010**, *87*, 2574–2580. [CrossRef]
19. Fueyo, N.; Sanz, Y.; Rodrigues, M.; Montañés, C.; Dopazo, C. High resolution modelling of the on-shore technical wind energy potential in Spain. *Wind Energy* **2010**, *13*, 717–726. [CrossRef]
20. Hasager, C.B.; Barthelmie, R.J.; Christiansen, M.B.; Nielsen, M.; Pryor, S. Quantifying offshore wind resources from satellite wind maps: study area the North Sea. *Wind Energy* **2006**, *9*, 63–74. [CrossRef]
21. Doubrawa, P.; Barthelmie, R.J.; Pryor, S.C.; Hasager, C.B.; Badger, M.; Karagali, I. Satellite winds as a tool for offshore wind resource assessment: The Great Lakes Wind Atlas. *Remote Sens. Environ.* **2015**, *168*, 349–359. [CrossRef]
22. Carvalho, D.; Rocha, A.; Santos, C.S.; Pereira, R. Wind resource modelling in complex terrain using different mesoscale–microscale coupling techniques. *Appl. Energy* **2013**, *108*, 493–504. [CrossRef]
23. Carvalho, D.; Rocha, A.; Gómez-Gesteira, M.; Santos, C. A sensitivity study of the WRF model in wind simulation for an area of high wind energy. *Environ. Model. Softw.* **2012**, *33*, 23–34. [CrossRef]
24. Carvalho, D.; Rocha, A.; Gómez-Gesteira, M.; Santos, C.S. Sensitivity of the WRF model wind simulation and wind energy production estimates to planetary boundary layer parameterizations for onshore and offshore areas in the Iberian Peninsula. *Appl. Energy* **2014**, *135*, 234–246. [CrossRef]
25. Carvalho, D.; Rocha, A.; Gómez-Gesteira, M.; Santos, C.S. Comparison of reanalyzed, analyzed, satellite-retrieved and NWP modelled winds with buoy data along the Iberian Peninsula coast. *Remote Sens. Environ.* **2014**, *152*, 480–492. [CrossRef]
26. Carvalho, D.; Rocha, A.; Gómez-Gesteira, M.; Santos, C.S. WRF wind simulation and wind energy production estimates forced by different reanalyses: Comparison with observed data for Portugal. *Appl. Energy* **2014**, *117*, 116–126. [CrossRef]
27. Carvalho, D.; Rocha, A.; Gómez-Gesteira, M.; Santos, C.S. Offshore wind energy resource simulation forced by different reanalyses: Comparison with observed data in the Iberian Peninsula. *Appl. Energy* **2014**, *134*, 57–64. [CrossRef]
28. Guerrero-Villar, F.; Dorado-Vicente, R.; Medina-Sánchez, G.; Torres-Jiménez, E. Alternative Calibration of Cup Anemometers: A Way to Reduce the Uncertainty of Wind Power Density Estimation. *Sensors* **2019**, *19*, 2029. [CrossRef]
29. Farkas, Z. Considering air density in wind power production. *arXiv* **2011**, arXiv:1103.2198.
30. Collins, J.; Parkes, J.; Tindal, A. Short term studies for utility-scale wind farms. The power model challenge. *Wind Eng.* **2009**, *33*, 247–257. [CrossRef]
31. Dahmouni, A.; Salah, M.B.; Askri, F.; Kerkeni, C.; Nasrallah, S.B. Assessment of wind energy potential and optimal electricity generation in Borj-Cedria, Tunisia. *Renew. Sustain. Energy Rev.* **2011**, *15*, 815–820. [CrossRef]
32. Svenningsen, L. *Power Curve Air Density Correction and Other Power Curve Options in WindPRO*; Technical report; EMD International A/S: Aalborg, Denmark, 2010. Available online: www.emd.dk/files/windpro/WindPRO_Power_Curve_Optionspdf (accessed on 15 May 2019).

33. Ulazia, A.; Sáenz, J.; Ibarra-Berastegui, G. Sensitivity to the use of 3DVAR data assimilation in a mesoscale model for estimating offshore wind energy potential. A case study of the Iberian northern coastline. *Appl. Energy* **2016**, *180*, 617–627. [CrossRef]
34. Ulazia, A.; Sáenz, J.; Ibarra-Berastegui, G.; González-Rojí, S.J.; Carreno-Madinabeitia, S. Using 3DVAR data assimilation to measure offshore wind energy potential at different turbine heights in the West Mediterranean. *Appl. Energy* **2017**, *208*, 1232–1245. [CrossRef]
35. Yamaguchi, A.; Ishihara, T. Assessment of offshore wind energy potential using mesoscale model and geographic information system. *Renew. Energy* **2014**, *69*, 506–515. [CrossRef]
36. Pourrajabian, A.; Mirzaei, M.; Ebrahimi, R.; Wood, D. Effect of air density on the performance of a small wind turbine blade: A case study in Iran. *J. Wind Eng. Ind. Aerodyn.* **2014**, *126*, 1–10. [CrossRef]
37. Soraperra, G. Design of wind turbines for non-standard air density. *Wind Eng.* **2005**, *29*, 115–128. [CrossRef]
38. Elosegui, U.; Egana, I.; Ulazia, A.; Ibarra-Berastegi, G. Pitch angle misalignment correction based on benchmarking and laser scanner measurement in wind farms. *Energies* **2018**, *11*, 3357. [CrossRef]
39. Esteban, M.; Leary, D. Current developments and future prospects of offshore wind and ocean energy. *Appl. Energy* **2012**, *90*, 128–136. [CrossRef]
40. Danook, S.H.; Jassim, K.J.; Hussein, A.M. The impact of humidity on performance of wind turbine. *Case Stud. Therm. Eng.* **2019**, *14*, 100456. [CrossRef]
41. Jung, C.; Schindler, D. The role of air density in wind energy assessment—A case study from Germany. *Energy* **2019**, *171*, 385–392. [CrossRef]
42. Dee, D.P.; Uppala, S.M.; Simmons, A.J.; Berrisford, P.; Poli, P.; Kobayashi, S.; Andrae, U.; Balmaseda, M.A.; Balsamo, G.; Bauer, P.; et al. The ERA-Interim reanalysis: Configuration and performance of the data assimilation system. *Q. J. R. Meteorol. Soc.* **2011**, *137*, 553–597. [CrossRef]
43. Rabanal, A.; Ulazia, A.; Ibarra-Berastegi, G.; Sáenz, J.; Elosegui, U. MIDAS: A Benchmarking Multi-Criteria Method for the Identification of Defective Anemometers in Wind Farms. *Energies* **2019**, *12*, 28. [CrossRef]
44. Aniskevich, S.; Bezrukovs, V.; Zandovskis, U.; Bezrukovs, D. Modelling the spatial distribution of wind energy resources in Latvia. *Latvian J. Phys. Tech. Sci.* **2017**, *54*, 10–20. [CrossRef]
45. Sterl, S.; Liersch, S.; Koch, H.; van Lipzig, N.P.; Thiery, W. A new approach for assessing synergies of solar and wind power: Implications for West Africa. *Environ. Res. Lett.* **2018**, *13*, 094009. [CrossRef]
46. Camargo, L.R.; Gruber, K.; Nitsch, F. Assessing variables of regional reanalysis datasets relevant for modelling small-scale renewable energy systems. *Renew. Energy* **2019**, *133*, 1468–1478. [CrossRef]
47. Engelhorn, T.; Müsgens, F. How to estimate wind-turbine infeed with incomplete stock data: A general framework with an application to turbine-specific market values in Germany. *Energy Econ.* **2018**, *72*, 542–557. [CrossRef]
48. Hörsch, J. PyPSA-Eur: An Open Optimization Model of the European Transmission System (Dataset). 2017. Available online: https://github.com/FRESNA/pypsa-eur (accessed on 15 May 2019).
49. Allaerts, D.; Broucke, S.V.; van Lipzig, N.; Meyers, J. Annual impact of wind-farm gravity waves on the Belgian–Dutch offshore wind-farm cluster. *J. Phys.* **2018**, *1037*, 072006 [CrossRef]
50. Sáenz, J.; González-Rojí, S.J.; Carreno-Madinabeitia, S.; Ibarra-Berastegi, G. aiRthermo: Atmospheric Thermodynamics and Visualization. R package version 1.2.1; 2018. Available online: https://cran.r-project.org/web/packages/aiRthermo/index.html (accessed on 15 May 2019).
51. Sáenz, J.; González-Rojí, S.J.; Carreno-Madinabeitia, S.; Ibarra-Berastegi, G. Analysis of atmospheric thermodynamics using the R package aiRthermo. *Comput. Geosci.* **2019**, *122*, 113–119. [CrossRef]
52. Ulazia, A.; Ibarra-Berastegi, G.; Sáenz, J.; Gonzalez-Rojí, S.J.; Carreno-Madinabeitia, S. Seasonal correction of offshore wind energy potential due to air density: Case of the Iberian Peninsula. *Sustainability* **2019**, *11*, 3648. [CrossRef]
53. ECMWF. Part IV: Physical Processes. In *IFS Documentation CY41R2*; Number 4 in IFS Documentation; ECMWF: Reading, UK, 2016.
54. United States Committee on Extension to the Standard Atmosphere. *National Oceanic and Atmospheric Administration, Washington, DC (NOAA-S/T 76-15672): Supt. of Docs., US Gov Print Office (Stock No. 003-017-00323-0)*; United States Committee on Extension to the Standard Atmosphere: Washington, DC, USA, 1976.
55. International Electrical Commission. *Wind Turbines-Part 12-1: Power Performance Measurements of Electricity Producing Wind Turbines*; IEC 61400-12-1; IEC: Geneva, Switzerland, 2005.

56. Masters, G.M. *Renewable and Efficient Electric Power Systems*; John Wiley & Sons: Hoboken, NJ, USA, 2013.
57. Casati, B.; Wilson, L.; Stephenson, D.; Nurmi, P.; Ghelli, A.; Pocernich, M.; Damrath, U.; Ebert, E.; Brown, B.; Mason, S. Forecast verification: Current status and future directions. *Meteorol. Appl.* **2008**, *15*, 3–18. [CrossRef]
58. Moseley, S. From Observations to Forecasts–Part 12: Getting the most out of model data. *Weather* **2011**, *66*, 272–276. [CrossRef]
59. Accadia, C.; Mariani, S.; Casaioli, M.; Lavagnini, A.; Speranza, A. Sensitivity of precipitation study skill scores to bilinear interpolation and a simple nearest-neighbor average method on high-resolution verification grids. *Weather Forecast.* **2003**, *18*, 918–932. [CrossRef]
60. Borge, R.; Alexandrov, V.; Del Vas, J.J.; Lumbreras, J.; Rodriguez, E. A comprehensive sensitivity analysis of the WRF model for air quality applications over the Iberian Peninsula. *Atmos. Environ.* **2008**, *42*, 8560–8574. [CrossRef]
61. Jiménez, P.A.; Dudhia, J. Improving the representation of resolved and unresolved topographic effects on surface wind in the WRF model. *J. Appl. Meteorol. Climatol.* **2012**, *51*, 300–316. [CrossRef]
62. Soares, P.M.; Cardoso, R.M.; Miranda, P.M.; de Medeiros, J.; Belo-Pereira, M.; Espirito-Santo, F. WRF high resolution dynamical downscaling of ERA-Interim for Portugal. *Clim. Dyn.* **2012**, *39*, 2497–2522. [CrossRef]
63. Lei, M.; Shiyan, L.; Chuanwen, J.; Hongling, L.; Yan, Z. A review on the studying of wind speed and generated power. *Renew. Sustain. Energy Rev.* **2009**, *13*, 915–920. [CrossRef]
64. NWTC Information Portal (FAST). 2019. Available online: https://nwtc.nrel.gov/FAST (accessed on 10 March 2019).
65. Kecskemety, K.M.; McNamara, J.J. Influence of wake dynamics on the performance and aeroelasticity of wind turbines. *Renew. Energy* **2016**, *88*, 333–345. [CrossRef]
66. Guntur, S.; Jonkman, J.; Sievers, R.; Sprague, M.A.; Schreck, S.; Wang, Q. A validation and code-to-code verification of FAST for a megawatt-scale wind turbine with aeroelastically tailored blades. *Wind Energy Sci. Discuss.* **2017**, *2*, 1389738. [CrossRef]
67. Guntur, S.; Jonkman, J.; Schreck, S.; Jonkman, B.; Wang, Q.; Sprague, M.; Hind, M.; Sievers, R. *FAST v8 Verification and Validation for a Megawatt-Scale Wind Turbine with Aeroelastically Tailored Blades*; Technical report; National Renewable Energy Lab. (NREL): Golden, CO, USA, 2016.
68. Cyranoski, D. Renewable energy: Beijing's windy bet. *Nat. News* **2009**, *457*, 372–374. [CrossRef] [PubMed]